Enhanced ionization of the molecular ion H_2^+ in intense laser and static magnetic fields

André D. Bandrauk and Hui Zhong Lu
Laboratoire de Chimie Théorique, Faculté des Sciences, Université de Sherbrooke, Sherbrooke, Quebec, Canada J1K 2R1
(Received 18 May 2000; published 12 October 2000)

The three-dimensional time-dependent Schrödinger equation is solved exactly for the H_2^+ molecular ion as a function of internuclear distance R in a short intense laser field pulse and a static magnetic field, parallel to the internuclear axis, using a numerical integration method. Previous calculations of laser-induced ionization in this ion for zero magnetic field [Phys. Rev. A **48**, 3837 (1993); **52**, 2511 (1995)] demonstrated the phenomenon of charge-resonance-enhanced ionization (CREI) at critical distances R_c, due to Stark displacements of the lowest unoccupied molecular orbital (LUMO) above internal proton Coulomb and static laser field barriers. The presence of the magnetic field allows for controlling the energy displacements of the LUMO and consequently control of CREI, thus confirming CREI as a quasistatic electron tunneling process in the nonsymmetric double-well potential created by protons and a laser field.

PACS number(s): 42.50.Hz, 32.60.+i

I. INTRODUCTION

Dissociation of molecular ions by strong static electric and magnetic fields was initiated in the 1960's, and motivated by possible applications to particle accelerators and fusion devices [1]. It was shown then that the static electric fields of the order of 1 V/Å would severely distort molecular potentials, thus inducing field dissociation [1–3]. Intense magnetic fields, on the other hand, predicted that one can stabilize molecular ions, and even change their geometry as in the case of H_3^+ in some stars [4]. Current laser technology provides for the creation of intense laser pulses whose peak intensities approach the atomic unit of intensity $I_0 = cE_0^2/4\pi = 3.5\times10^{16}\,\mathrm{W/cm^2}$ corresponding to the atomic unit (a.u.) of electric field $E_0 = e^2/a_0^2 = 5\times10^9\,\mathrm{V/cm}$, where $a_0 = 1$ a.u. $= 0.52\times10^{-8}$ cm. The atomic unit of the magnetic field is $B_0 = 2.35\times10^9$ G, and has not yet been achieved, but pulsed fields of $10^{-2}B_0$ are now attainable [5].

In the present work we shall investigate the effect of such intense magnetic fields on a nonperturbative phenomenon occurring in laser-molecule interaction: *charge-resonance enhanced ionization* (CREI), first discovered in numerical solutions of the time-dependent Schrödinger equation (TDSE), for H_2^+ as a function of internuclear distance R [6,7]. It was shown that ionization rate maxima occur at large critical distances R_c, and that these maxima can be explained as ionization of the electron from a Stark shifted lowest unoccupied molecular orbital (LUMO), the $1\sigma_u$ orbital in the case of H_2^+. This LUMO finds itself displaced over and above the net static Coulomb barrier created by the protons and the peak electric field of the laser in a narrow region around the critical distance R_c. For H_2^+ and other odd electron diatomics, R_c has been shown to be $\sim 4/I_p$ and $5/I_p$ for H_3^{2+} [8,9], where I_p is the ionization potential (e.g., 0.5 a.u. for a three-dimensional H atom). This LUMO model has also been confirmed to hold for nonlinear molecular ions [10]. Such a mechanism of over-barrier ionization was suggested as early as 1989 in Ref. [11], based on the intuitive picture of partial localization of the ionizing electron in either upper or lower wells created by the net nuclear Coulomb plus laser field potentials. Based on this picture, an estimate of $R_c \simeq 3/I_p$ is obtained by considering that electron localization occurs when the quasidegenerate valence molecular orbitals fall below the internal field free Coulomb barrier [11,12]. This picture neglects the important Stark shifts of the highest occupied molecular orbital (HOMO) and the (LUMO) which are coupled by the large radiative interaction $\mu(R)E$ respectively. $\mu(R) = R/2$ for H_2^+, and is due to a charge resonance (CR), electron transfer between the two quasidegenerate orbitals at large R, a concept originally introduced by Mulliken to explain intense electronic absorption bands in symmetric molecule [13]. We have shown previously that it is the laser excitation of the LUMO which populates it continuously as the laser changes phase [14,15]. In actual calculations, no localization of the electron in the LUMO is observed [7–9] due to the rapid ionization. The relevant physical scales are the photon frequency ($3\times10^{14}\,\mathrm{s^{-1}}$ at $\lambda = 1064$ nm), ionization rates [7–12] (10^{13}–$10^{14}\,\mathrm{s^{-1}}$) and the zero-field tunneling frequency of the electron between the two wells: $\hbar\omega_t = \varepsilon_{1\sigma_u}(R) - \varepsilon_{1\sigma_g}(R)$ which is R dependent. At $R = 6$ a.u. in the case of H_2^+, $\varepsilon_{1\sigma_u} - \varepsilon_{1\sigma_g} = 0.48$ eV, $\simeq$ $4000\,\mathrm{cm^{-1}}$, then $\omega_t \simeq 10^{14}\,\mathrm{s^{-1}}$ [16]. Thus all three time scales—photon, ionization and internal tunneling—are of the same order. This is the main difference between atoms and molecules. Thus for atoms direct field-induced static ionization rates over barriers are a useful concept for understanding low-frequency, high-intensity atomic multiphoton processes [17–19]. Symmetric molecular ions with H_2^+ as the prototype have important CR transitions, e.g., through the $1\sigma_g$-$1\sigma_u$ molecular orbitals in H_2^+ which act as doorway states. This makes molecules different from atoms, due to the presence of the nonlinear phenomenon: CREI [6–10].

In the present work, we develop a numerical scheme for calculating ionization rates of H_2^+ in the presence of an intense magnetic field. We have previously shown that magnetic fields parallel to the laser field and the molecular axis can extend high-order harmonic generation to higher order than without a magnetic field, due to the confinement and recollision of the electron with the parent ion [20]. In the present case, we present a more accurate three-dimensional (3D) numerical method which will be used later for a previous proposed scheme of controlling harmonics in the presence of magnetic fields [21]. In the present work we show

that strong magnetic fields allow for the control of CREI in H_2^+ via the variation of the energy of its LUMO, thus confirming its role as the doorway state for multiphoton ionization of molecular ions [7–10].

II. TIME-DEPENDENT HAMILTONIAN AND NUMERICAL METHOD

We have previously demonstrated the control of high-order harmonic generation (HOHG) by a static magnetic field for a 3D H_2^+ molecular ion in both a linearly polarized laser field and an ultrastrong static magnetic field parallel to the laser polarization and molecular axis [20], and a 2D model of the hydrogen atom in both a circularly polarized laser field and a magnetic field perpendicular to the laser-field polarization [21]. Recent work on HOHG in atoms in the presence of combinations of static electric and magnetic fields has demonstrated extension of the harmonic order and further confirmation of the electron-ion recollision model for HOHG [22].

The total 3D *electronic* Hamiltonian of H_2^+ for fixed nuclei at a distance R in a magnetic field B and laser field $E(t)\cos(\omega t)$, both collinear and parallel to the z axis (the internuclear axis), is given in cylindrical coordinates $\rho=(x^2+y^2)^{1/2}z$ by

$$
\begin{aligned}
i\frac{\partial\psi(z,\rho,t)}{\partial t}=&-\left(\frac{2m_p+1}{4m_p}\right)\left[\frac{\partial^2}{\partial\rho^2}+\frac{1}{\rho}\frac{\partial}{\partial\rho}+\frac{\partial^2}{\partial z^2}\right]\psi(z,\rho,t)\\
&-\left[\frac{1}{[(z\pm R/2)^2+\rho^2]^{1/2}}\right]\psi(z,\rho,t)\\
&+\left[\left(\frac{2m_p+2}{2m_p+1}\right)zE(t)\cos(\omega t)\right.\\
&\left.+\frac{\beta^2}{2}\rho^2-\beta\right]\psi(z,\rho,t). \qquad (1)
\end{aligned}
$$

This corresponds to a molecule *aligned* by the laser field, as expected for such high intensities [10]. In the electronic Hamiltonian [Eq. (1)], we have used atomic units (a.u.) ($e=\hbar=m_e=1$) $\beta=B/B_0$ where $B_0=2.35\times10^9$ G. This Hamiltonian is the exact three-body Hamiltonian for fixed protons aligned with the laser and magnetic fields (obtained after separation of the center of mass motion [1]). Furthermore we have kept the last term $-\beta$, the spin-Zeeman effect needed to obtain the exact initial ground state [23]. Hamiltonian (1) does not contain the orbital Zeeman term βl_z, [1], since our initial electronic state is the zero orbital momentum state $1\sigma_g$, and the laser field $E(t)$ is linearly polarized [20,21] along the z axis. The second term is the Coulomb potential from the two protons on the z axis at $\pm R/2$. $\beta^2\rho^2/2$ is the diamagnetic energy term acting as a parabolic barrier (magnetic bottle) in the ρ direction, giving rise to magnetic confinement in that direction. The parameter that characterizes the magnetic confinement is the Landau radius defined by $R_L=(2/\beta)^{1/2}$. Thus for $\beta=10^{-2}B_0$ or $B=2.35\times10^7$ G, $R_L=14$ a.u. This is the size of the circular radius for electron harmonic motion in the ρ direction (around the z axis) induced by the magnetic field.

The first numerical solution of the H_2^+ TDSE in a laser field was obtained for *aligned* and *fixed* nuclei using an expansion in terms of eigenfunctions of the cylindrical Laplacian, $\partial^2/\partial\rho^2+(1/\rho)\partial/\partial\rho$ [24]. These eigenfunctions which are Bessel functions of zero order, reduced the dimensionality of Eq. (1) to 2, i.e., z and R, and furthermore removed the Coulomb singularity due to the electron proton interaction at $z=\pm R/2$ and $\rho=0$. However, this Coulomb potential becomes a large matrix in such a basis set, thus necessitating a high-order split-operator method [25] for solving the TDSE for static nuclei [6,7], but also with moving nuclei [26]. We have also used previously three-dimensional Cartesian finite-element (FE) methods [27] for molecular TDSE's. Such basis sets have the desirable advantage of being very flexible, spanning bound and continuum states simultaneously. The price for such flexibility is that since FE bases are local, a large number of bases are required to cover adequately the global behavior of the exact time-dependent solution. Another choice is to solve Eq. (1) in prolate spheroidal coordinates which is separable in zero field. Then doing a complex energy Floquet expansion with Laguerre and Legendre polynomial bases (the eigenstates of the zero field problem), one can extract field-induced shifts and widths corresponding to adiabatic field conditions [28].

Another approach is to use adaptive space coordinate or grid methods, which look particularly promising for density-functional approaches due to the reduced dimensionality of the electronic problems [29]. Recently Kawata and Kono developed such an adaptive grid representation [30] for H_2^+, i.e., using a generalized cylindrical coordinate system $\rho=f(\rho)$ and $z=g(\rho)$ where f and g are polynomials, they have improved on the treatment of the wave function near the origin, which can create considerable difficulty in (uniform) discretized grid approaches [20].

In the present work we adopt a more general nonlinear coordinate transformation in order to obtain a variable, nonuniform grid, dense at singularities and equidistant asymptotically. Thus we choose the general transformation $\rho=T(\tilde{\rho})$, $z=T(\tilde{z})$ with

$$
T(u)=u\left(\frac{u^n+sp^n}{u^n+p^n}\right), \qquad (2)
$$

where n is an even integer, $p\geqslant0$ representing the domain of grid refinement, and $0\leqslant s\leqslant1$ is set to be the minimum of DT/Du. This is necessary to insure that the grid is concentrated near the singularities. The properties of this transformation are (setting primes equal to derivatives)

$$
T(u)=1+(1-s)\frac{(n-1)[1+(u/p)^n]-n}{[1+(u/p)^n]^2}, \qquad (3)
$$

$$
T'(0)=s,\quad T'(\infty)=1,
$$

$$
T'(p)=1+\frac{(1-s)(n-2)}{4}. \qquad (4)
$$

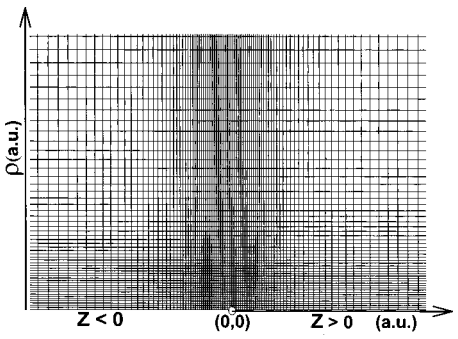

FIG. 1. Adaptive grid used to solve the TDSE, [Eq. (1)], with variable coordinates $\tilde{\rho}$ and $\tilde{z}$ [Eq. (2)]. Grid points become equidistant at large ρ and z.

For $n=4$, $s=0.2$, and $p>0$, in Fig. 1 we illustrate an example of this new adaptive grid for cylindrical coordinates.

As a result of the normalization condition

$$\int\int \rho|\psi|^2\, d\rho\, dz = \int\int \rho|\tilde{\psi}|^2\, d\tilde{\rho}\, d\tilde{z} = 1, \tag{5}$$

the new transformed function becomes

$$\tilde{\psi} = [T'(\tilde{\rho})T'(\tilde{z})]^{1/2}\psi, \tag{6}$$

and the new Laplacian in Eq. (1) is transformed according to

$$\begin{aligned}
\frac{1}{\rho}\frac{\partial\psi}{\partial\rho} &\rightarrow \frac{1}{(T')^{1/2}}\frac{\partial}{\rho\,\partial\tilde{\rho}}\frac{\tilde{\psi}}{(T')^{1/2}},\\
\frac{\partial^2\psi}{\partial\rho^2} &\rightarrow \frac{1}{(T')^{1/2}}\frac{\partial}{\partial\tilde{\rho}}\frac{1}{T'}\frac{\partial}{\partial\tilde{\rho}}\frac{\tilde{\psi}}{(T')^{1/2}},\\
\frac{\partial^2\psi}{\partial z^2} &\rightarrow \frac{1}{(T')^{1/2}}\frac{\partial}{\partial\tilde{z}}\frac{1}{T'}\frac{\partial}{\partial\tilde{z}}\frac{\tilde{\psi}}{(T')^{1/2}}.
\end{aligned} \tag{7}$$

Each differential operator in Eqs. (7) is then discretized by a seven-point difference formula which has fifth-order accuracy as compared to the three-point method in Ref. [20] which gives second-order accuracy only. It was recently demonstrated that such three-point formulas can be made exponentially convergent by a variational formulation [31]. However, for the present time-dependent problem, where one must iterate the spatial discretization in time, such a procedure is time consuming; it has not yet been implemented here, but is investigated further for Cartesian coordinate [32].

We impose the following boundary conditions:

$$\tilde{\psi} = 0 \quad \text{at} \quad \rho = \rho_{\max} \quad \text{and} \quad |z| = z_{\max}, \tag{8}$$

$$\frac{\partial\tilde{\psi}}{\partial\tilde{\rho}} = 0 \quad \text{at} \quad \rho = 0. \tag{9}$$

$\rho_{\max}$ and $z_{\max}$ are the maximum sizes of the grid, and annihilation of the wave function at those limits is obtained by applying an artificial absorber of the type $\cos^{1/8}(u)$ [20]. Condition (9) at the ρ origin is equivalent to the symmetry condition $\psi(-\rho)=\psi(+\rho)$ imposed previously by Zuo *et al.* [20] in the standard (uniform) grid formulation of the problem. However, this necessitated doubling the grid domain to $[-\rho_{\max},\rho_{\max}]$, whereas in the present adaptive (nonuniform) grid method the boundary condition is directly applied. Two choices are available for imposing this boundary condition: at the nuclei or between the nuclei. It is found that one cannot efficiently impose the boundary choice at the nuclei due to Coulomb singularities, but one must opt for positions between the nuclei [32] for most efficient convergence.

For the time propagation, we choose an alternating direction implicit method for all Laplacians terms, since fast Fourier transform methods for nonuniform grids are inefficient in general. We use a direct exponentiation method for the 3D Coulomb potential in Eq. (1). Each time propagation step for the length $zE(t)$ gauge is chosen as

$$\begin{aligned}
\tilde{\psi}(t+\delta t) = &\left[1+i\frac{\delta t}{4}A_\rho\right]^{-1}\exp\left(-i\frac{\delta t}{4}A_v\right)\left[1-i\frac{\delta t}{4}A_\rho\right]\\
&\times\left(\left[1+i\frac{\delta t}{4}Az\right]^{-1}\exp\left(-i\frac{\delta t}{4}A_v\right)\left[1-i\frac{\delta t}{4}Az\right]\right)^2\\
&\times\left[1+i\frac{\delta t}{4}A_\rho\right]^{-1}\exp\left(-i\frac{\delta t}{4}A_v\right)\\
&\times\left[1-i\frac{\delta t}{4}A_\rho\right]\tilde{\psi}(t),
\end{aligned} \tag{10}$$

where

$$\begin{aligned}
A_\rho = -\frac{2m_p+1}{4m_p}\Bigg[&\frac{1}{(\rho')^{1/2}}\frac{\partial}{\partial\tilde{\rho}}\frac{1}{\rho'}\frac{\partial}{\partial\tilde{\rho}}\frac{1}{(\rho')^{1/2}}\\
&+\frac{1}{\rho(\rho')^{1/2}}\frac{\partial}{\partial\tilde{\rho}}\frac{1}{(\rho')^{1/2}}+\left(\frac{\beta^2}{2}\rho^2-\beta\right)\Bigg],
\end{aligned} \tag{11}$$

$$\begin{aligned}
A_z = -\frac{2m_p+1}{4m_p}\Bigg[&\frac{1}{(z')^{1/2}}\frac{\partial}{\partial\tilde{z}}\frac{1}{z'}\frac{\partial}{\partial\tilde{z}}\frac{1}{(z')^{1/2}}\\
&+\left(\frac{2m_p+2}{2m_p+1}\right)E(t)z\cos(\omega t)\Bigg],
\end{aligned} \tag{12}$$

$$A_v = [(z\pm R/2)^2+\rho^2]^{-1/2}. \tag{13}$$

One can also propagate the TDSE in the velocity gauge by the unitary (gauge) transformation [3]

$$\begin{aligned}
\psi \rightarrow \psi\exp\Bigg\{&-i\frac{2m_p+1}{4m_p}\left[\int_0^t\left(\int_0^s E(\tau)d\tau\right)^2 ds\right]\\
&-iz\int_0^t E(s)ds\Bigg\},
\end{aligned} \tag{14}$$

which gives the new TDSE,

$$i\frac{\partial\psi}{\partial t} = H_0\psi + i\left[\frac{2m_p+1}{2m_p}\int_0^t E(s)ds\right]\frac{\partial\psi}{\partial z}, \tag{15}$$

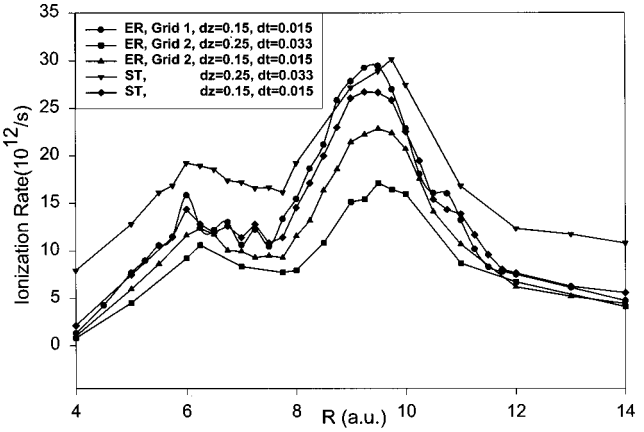

FIG. 2. Ionization rates as a function of R in the length gauge (ER) [Eq. (10)] and space translation (ST) gauge [Eq. (18)] for two different grid point distributions, grids 1 and 2 (see text), at $\lambda = 1064$ nm and $I = 10^{14}$ W/cm^2.

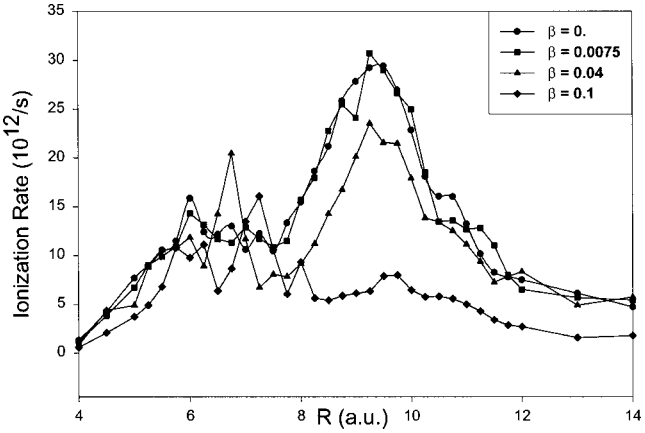

FIG. 3. Ionization rates as a function of R at $\lambda = 1064$ nm and $I = 10^{14}$ W/cm^2 for different magnetic fields $\beta = B/B_0$ in the space translation gauge.

with H_0 the field-free $[E(t)=0]$ Hamiltonian. This is nothing but the Coulomb gauge, since $\hat{p} = i\partial/\partial z$ [3]. Changing variables once more to a Lagrangian moving system,

$$u = z + \frac{2m_p+1}{2m_p}\int_0^t ds \int_0^s E(\tau)\,d\tau, \tag{16}$$

gives the function $\psi(\rho,u,t)$ which satisfies the TDSE

$$i\frac{\partial\psi}{\partial t} = H_0(u)\psi, \tag{17}$$

where the laser field is now included in H_0 through the displaced coordinates u. This is equivalent to the space translation, representation [3] generally used for high frequencies, but is also known as a Lagrangian system in classical fluid mechanics [32]. This allows for a simplification of the propagation by the scheme

$$\begin{aligned}\tilde{\psi}(t+\delta t) = &\left[1 + i\frac{\delta t}{4}A_\rho\right]^{-1}\exp\left(-i\frac{\delta t}{4}A_v\right)\left[1 - i\frac{\delta t}{4}A_\rho\right]\\ &\times\left[1 + i\frac{\delta t}{2}A_u\right]^{-1}\exp\left(-i\frac{\delta t}{2}A_v\right)\\ &\times\left\{1 - i\frac{\delta t}{2}A_u\left[1 + i\frac{\delta t}{4}A_\rho\right]^{-1}\right.\\ &\left.\times\exp\left(-i\frac{\delta t}{4}A_\nu\right)\left[1 - i\frac{\delta t}{4}A_\rho\right]\tilde{\psi}(t)\right\},\end{aligned} \tag{18}$$

where

$$A_u = -\frac{2m_p+1}{4m_p}\left[\frac{1}{(u')^{1/2}}\frac{\partial}{\partial\tilde{u}}\frac{1}{u'}\frac{\partial}{\partial\tilde{u}}\frac{1}{(u')^{1/2}}\right]. \tag{19}$$

This results in a moving adaptive grid, since u is time dependent [Eq. (16)], and hence known as a Lagrangian coordinate system [32].

In Fig. 2, we illustrate for a zero magnetic field ($\beta = 0$), the convergence of this integration method for the two gauges: length (ER) [Eq. (10)] and space translation (ST) [Eq. (18)], and two different grids 1 and 2. The ionization rate of H_2^+ for a laser field of wavelength $\lambda = 1064$ nm, intensity $I = 10^{14}$ W/cm^2 (a five-cycle rise of the pulse) exhibits our previously published result: two maxima around $R = 6$ and 9.5 a.u., with rates exceeding that of the H atom ($R \to \infty$) by about one order of magnitude. A coarse grid $dz = 0.25$ a.u. and $dt = 0.033$ a.u. [t (a.u.) $= 2.42\times10^{-17}$ s] gives approximately a factor of 2 different between length (■) and ST (▼) gauges. The finer grid $dz = 0.15$ a.u. and $dt = 0.015$ a.u. shows near agreement between both gauges. We note that in the ST gauge, because of the moving coordinates, there is no advantage in specifying the position of the grid points. In the length gauge, as stated above, one can insist on placing certain grid points at the proton positions, where the Coulomb singularities occur (grid 2), whereas grid 1 in Fig. 2 corresponds to the case where the protons and zero function boundary condition do not coincide. It is clearly grid 1 (●), with grid points avoiding the singularities, which gives closer agreement between the two gauges. It is to be noted that ST results (♦, ▼) are very similar in spite of the finer grid for the case ♦ ($dz = 0.15$) and closest to the grid 1 results (●). We also emphasize that the ST method, which corresponds to a moving grid following the ionized electron at large distances, converges most rapidly due to its better approximation of the inherent physics at large distances.

In Fig. 3 we illustrate the same calculation as in Fig. 2 in the ST gauge, but now with different values of the magnetic field in a.u., $\beta = B/B_0$, where $B_0 = 2.35\times10^9$ G. The most evident result is the suppression of the ionization maximum around $R = 9.5$ a.u., whereas the first maximum at $R \cong 6.5$ a.u. exhibits new structure typical of resonances. We reiterate that all results are for 3D H_2^+ with both laser $[E(t)]$ and magnetic (B) fields parallel to the internuclear axes R or z. In Sec. III we interpret this ionization suppression in terms of magnetic field displacement of the LUMO energies, and we also illustrate the 3D nature of the electron wave function $\psi(z,\rho,R,t)$.

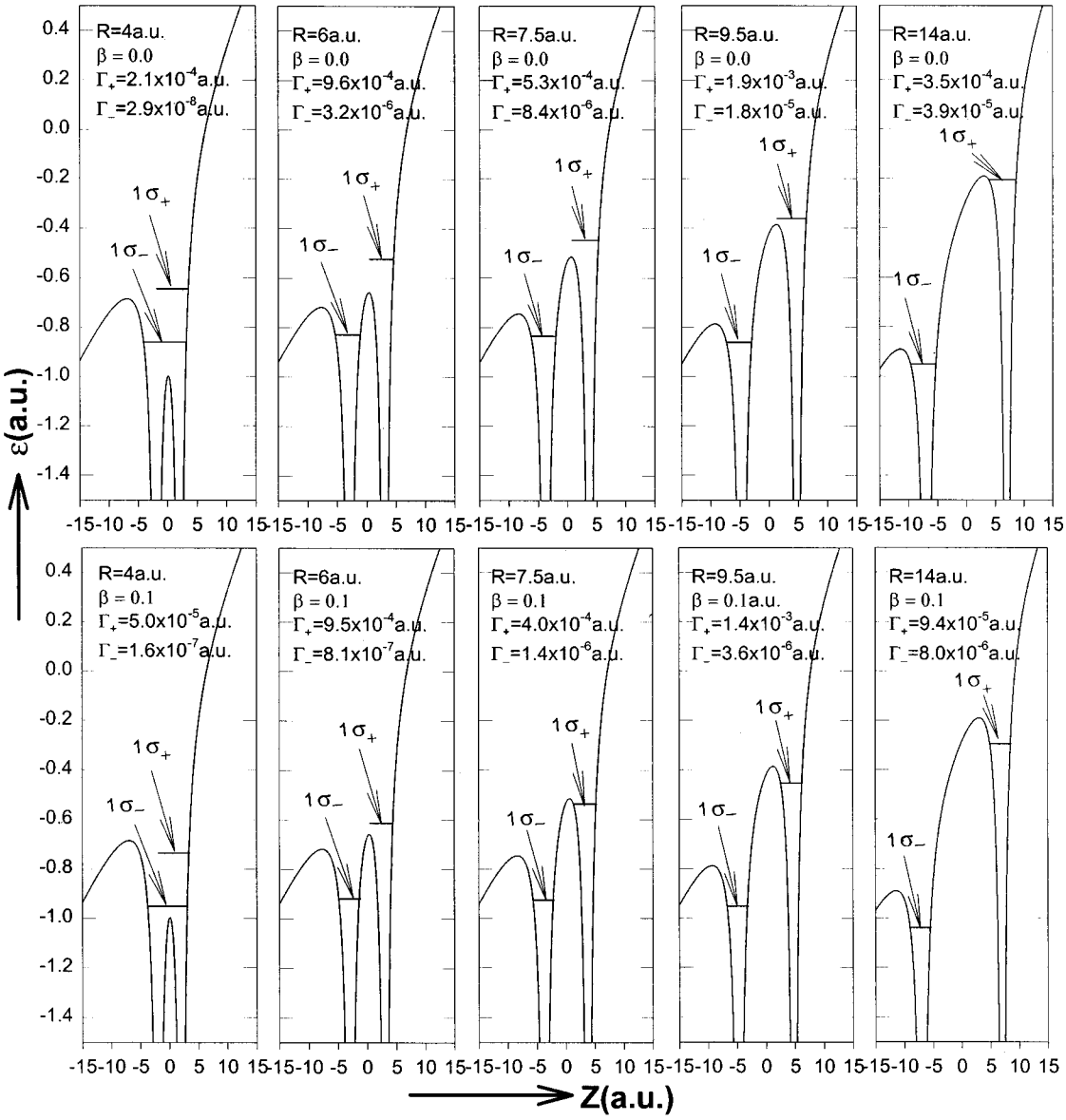

FIG. 4. Energies and widths $\Gamma_{\pm}$ of the LUMO ($1\sigma_+$) and the HOMO ($1\sigma_-$) at a static electric field $E=0.053$ a.u. ($I=10^{14}$ W/cm^2) and different magnetic fields $\beta=B/B_0$.

III. ENHANCED IONIZATION AND CHARGE-RESONANCE STATES

Symmetric molecular ions differ from atoms due to the presence of molecular CR states [3,13]. Such states are described by pairs of molecular orbitals of opposite symmetry which dissociate to the same atomic orbitals. Thus, for H_2^+, the HOMO is $1\sigma_g$, and the LUMO is $1\sigma_u$, in symmetry, with both dissociating to the $1s$ atomic orbital, resulting in a divergent transition moment $\mu(R)=R/2$. In a static field of strength E, this results in a large coupling $ER/2$ with the concomitant Stark displacement of the HOMO and LUMO by the energies $\mp$ER/2, respectively [7–9]. The resulting $1\sigma_g$ HOMO and $1\sigma_u$ LUMO are transformed into new orbitals $1\sigma_-$ and $1\sigma_+$, which approach the localized atomic $1s$ orbitals in either left or right potential wells of the new nonsymmetric double well created by the total proton Coulomb potential and static field energy E_z. This is illustrated in Fig. 4 for different magnetic-field strengths $\beta=0$ and 0.1 a.u. The energy levels $\varepsilon_{\pm}$ and widths Γ_+ were obtained by propagation of the TDSE [Eq. (1)] in a static electric field, $E=0.053$ a.u., corresponding to the intensity $I=10^{14}$ W/cm^2 (see Ref. [7] for details). In the present simulation, absorbing boundaries were applied in both ρ and z directions, whereas in Ref. [7] only absorption at the extremities of the z grid was applied. The results for a zero field, $\beta=0$ [Fig. 4(a)], are nearly identical, differing at most by 20%. As pointed out in Sec. II, the new LUMO, $1\sigma_+$ rapidly ionizes so that one can not speak of localization, as seen by the widths Γ_+. Thus at $R_c=9.5$ a.u., the maximum in ionization (Fig. 2), $\Gamma_+=2\times10^{-3}$ a.u.$=435\,\mathrm{cm}^{-1}$ or a lifetime $\tau=5\times10^{-12}\,\mathrm{s}/\Gamma(\mathrm{cm}^{-1})\cong10^{-14}$ s. Perusal of Fig. 4 shows that for internuclear distance $R\geqslant6$ a.u., the energy difference between the LUMO($1\sigma_+$) and HOMO($1\sigma_-$) in the field is indeed the Stark energy ER, and this is indepen-

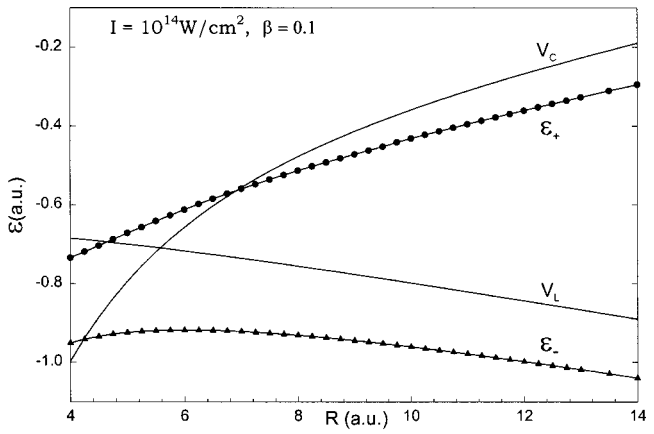

FIG. 5. Energies $\varepsilon_{\pm}$ of the LUMO $(1\sigma_{+})$ and the HOMO $(1\sigma_{-})$ for an electric field $E=0.053$ a.u. $(I=10^{14}\,\mathrm{W/cm^2})$ and a magnetic field $\beta=B/B_0$. V_c and V_l are the maxima of central and left barriers in Fig. 4.

dent of the magnetic-field strength. We note that this energy separation corresponds to the expected classical energy difference for an electron in a static field E at different proton sites separated by the distance R. This classical Stark effect was shown to be responsible for a new plateau in molecular HOHG, with generation efficiencies much larger than in atoms [6].

As one increases the magnetic field strength from $\beta=0$ to 0.1 $(2\times10^8\,\mathrm{G})$ (Fig. 3), one observes that the maximum in ionization rate is gradually suppressed and is displaced toward smaller distances R_c. Thus for $\beta=0.1$, $R_c\cong7.5$ a.u., in accordance with Fig. 4, which shows that at the higher magnetic-field strength, trapping of the $1\sigma_{+}$ orbital by the middle Coulomb barrier occurs at shorter distances. Thus the overall behavior is the large increase of ionization rate for $6\leqslant R\leqslant10$ a.u., with a rapid decrease outside this range for small magnetic field. At $\beta=0.1$, the maximum at $R_c\cong9.5$ a.u. is suppressed, and is displaced to shorter distances. We confirm this interpretation by examining Fig. 5, where the static E field energies of the LUMO, $\varepsilon_{+}(\bullet)$ and HOMO, $\varepsilon_{-}(\blacktriangle)$ are plotted as functions of R. In this figure we also show the maximum of the central barrier V_c and the left outer barrier V_l. Thus at $R\leqslant5$ a.u., the LUMO is trapped below the left barrier V_l, so it is completely localized in the molecule. At $R=5.7$ a.u., both barrier maxima are equal but the LUMO is delocalized, i.e., it is above both barriers. At $R\cong7$ a.u., we see that the LUMO is degenerate with the maximum of V_c, and is then trapped in the upper right well for $R>7$ a.u., in agreement with the ionization rate results illustrated in Fig. 3.

This simple interpretation of CREI in terms of quasistatic tunneling and overbarrier ionization at the peak of the laser field is nevertheless compounded by resonances, as pointed out in Ref. [28]. In Fig. 6 we illustrate the R dependence of the widths $\Gamma_{\pm}$ for $\beta=0$ and 0.1. The width of the HOMO, Γ_{-}, is clearly negligible, as that level is always trapped by the barriers in the asymmetric double well (Fig. 4). The width of the LUMO, $\Gamma_{+}(R)$, shows two maxima at $R=6$ and 9.7 a.u., corresponding to resonancelike effects through

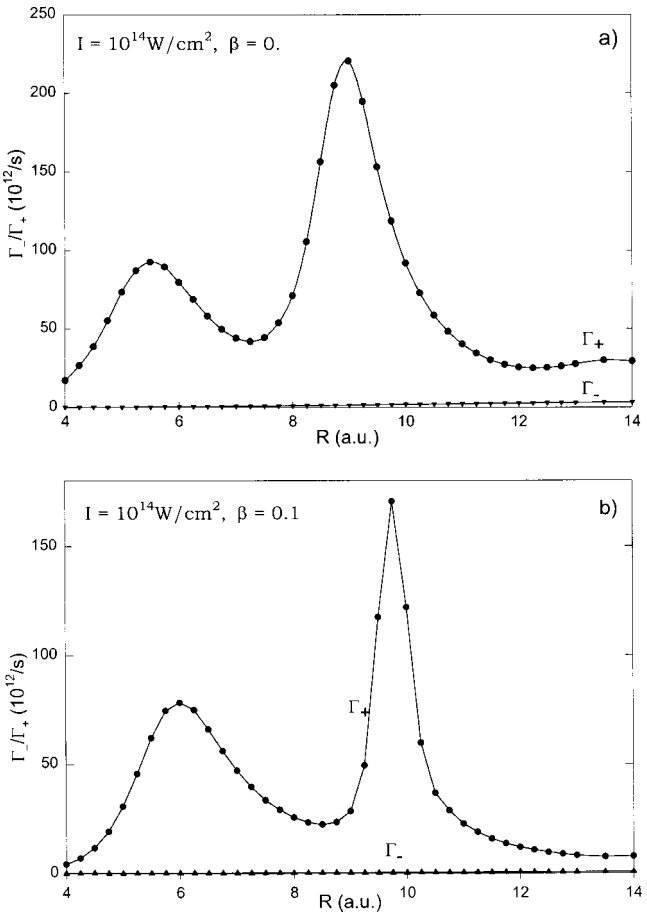

FIG. 6. Energy widths Γ of the HOMO (Γ_{+}) and the LUMO (Γ_{-}). (a) Zero magnetic field $(\beta=0)$. (b) $\beta=0.1$.

highly excited states of H_2^{+}. Figure 4 shows that such resonance effects do not dominate the ionization rate. Thus the maximum ionization rate at $\beta=0.1$ occurs around $R_c\cong7.5$ a.u. which agrees quite well with the simple overbarrier ionization image illustrated in Fig. 4.

In Figs. 7 $(\beta=0)$ and 8$(\beta=0.1)$ we illustrate the probability distribution $|\psi(z,\rho,R,t)|^2$ of the electron after 11.25 cycles of the field, which corresponds to a maximum of the field $E=0.053$ a.u. or the corresponding intensity $I=10^{14}\,\mathrm{W/cm^2}$. Four internuclear distances are depicted $R=6$, 7.5, 9.5, and 14 a.u., in order to illustrate the effect of the laser and magnetic fields on the wave-function evolution. For zero magnetic field (Fig. 7), $R=14$ a.u. shows atomiclike wave-function evolution, which can be interpreted as field-induced tunneling [17–19]. We note that at $R=6$ and 9.5 a.u., wave-function expansion in the transverse (ρ) direction becomes effective, especially at $R_c=9.5$ a.u., where the ionization maximum occurs (Fig. 3). The electron distribution at $R=9.5$ a.u. shows ionization occurring from both atoms, with excitation into large radius orbits at both nuclei. This we interpret as indicative of highly excited resonance states [32] as also suggested by the *ab initio* calculations [28].

Figure 8 illustrates the effect of a strong magnetic field, $\beta=0.1$ or $B=2.5\times10^8$ G. The expansion of the wavefunction is clearly suppressed by a magnetic (bottle) effect due to the diamagnetic term $\beta^2\rho^2/2$ [Eq. (1)]. Thus the maximum

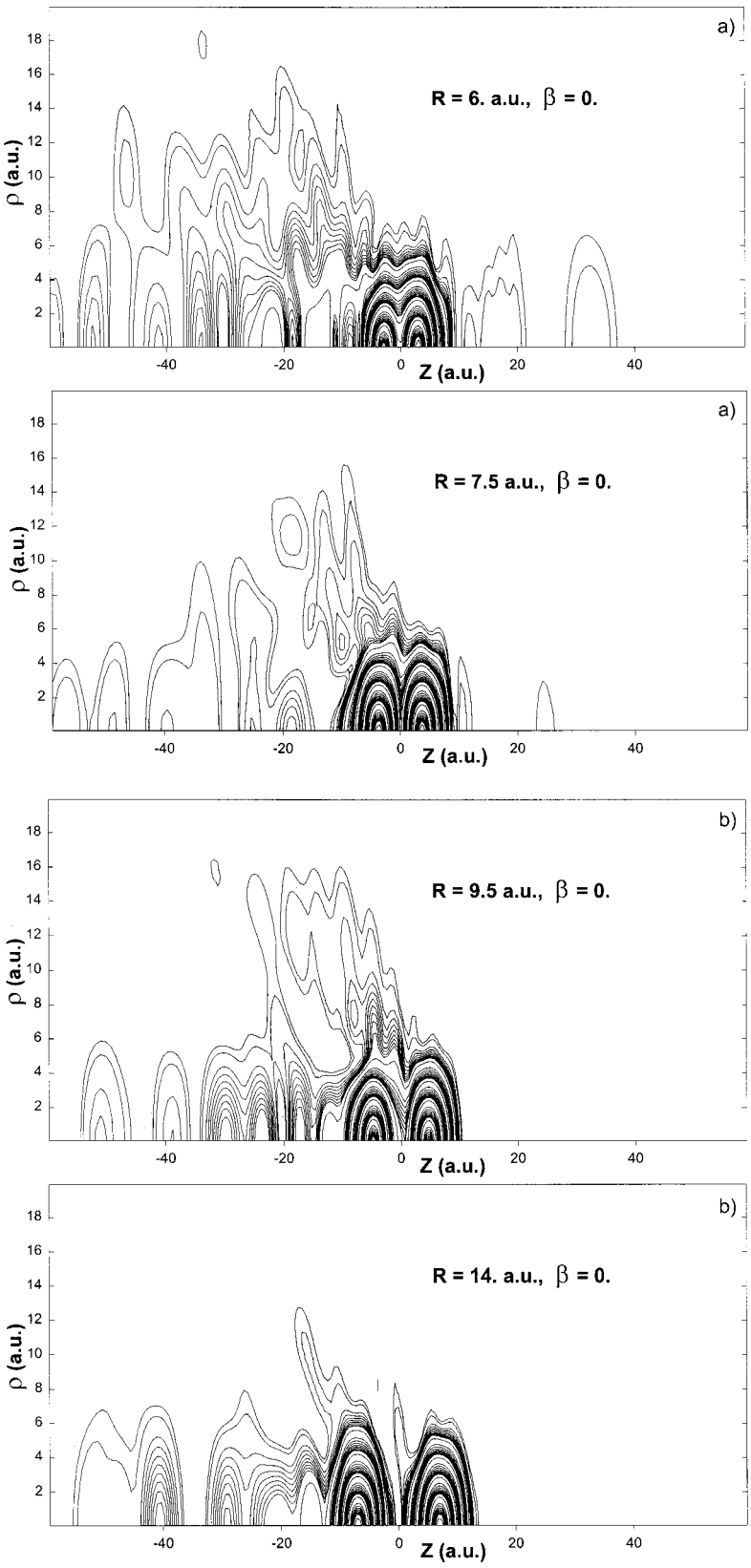

FIG. 7. Electron density $|\psi(z,\rho,R,t)|^2$ at $\beta=0$, $t=11.25$ cycles, $I=10^{14}\,\mathrm{W/cm^2}$, and $\lambda=1064\,\mathrm{nm}$. (a) $R=6$ and 7.5 a.u. (b) $R=9.5$ and 14 a.u.

extension into the ρ axis is about 10 a.u., as compared to 18 a.u. in the free magnetic-field ($\beta=0$) case (Fig. 7). As a result, excitation into highly excited states with a large radius is inhibited, e.g., at $R=9.5$ especially. The ionization is restricted to the magnetic field or equivalently the internuclear axis, thus making a 1D over barrier ionization dominant [33].

We therefore conclude that in molecules there are there regimes of ionization as a function of internuclear distance. As shown previously, these different regimes have a marked influence on HOHG and light scattering processes [6,14]. At

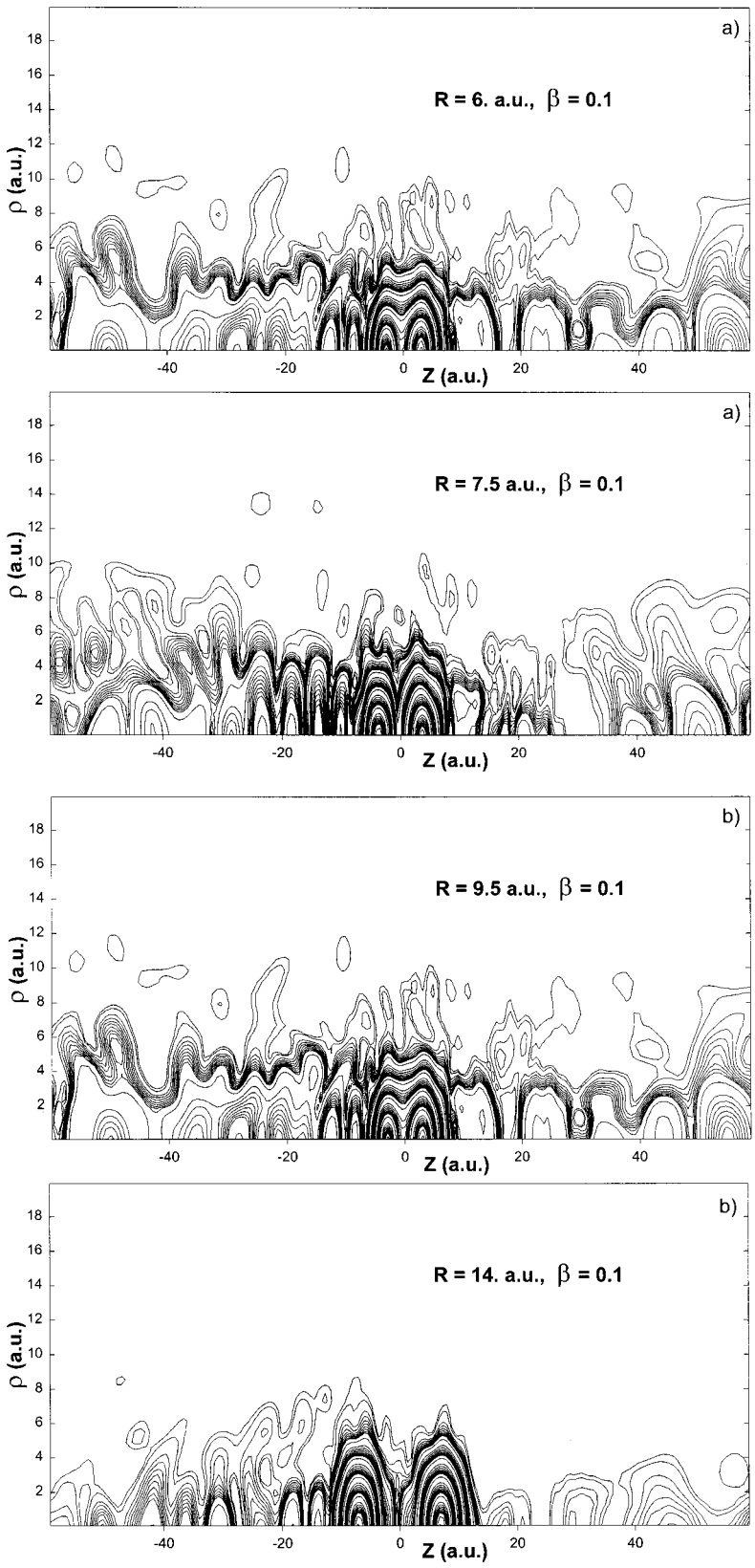

FIG. 8. Electron density $|\psi(z,\rho,R,t)|^2$ at $\beta = 0.1$, $t = 11.25$ cycles, $I = 10^{14}$ W/cm^2, and $\lambda = 1064$ nm. (a) $R = 6$ and 7.5 a.u. (b) $R = 9.5$ and 14 a.u.

small $R < R_c$, one has the atomic regime, since the ionization potential is large and the first excited state, the LUMO, can only be reached by a multiphoton excitation. In this regime, ADK tunneling ionization rates are adequate [34]. In the intermediate R region, e.g., photon resonances will become dominant and are partly responsible for the ionization peaks evident in Fig. 4 at $R \cong 6$ a.u. [6,14,27]. The region of large R is where the CREI mechanism via Stark displacement of the LUMO above barriers occurs up to the critical distance $R_c \cong 4/I_p$ for odd electron diatomic systems [8,9] and $5/I_p$ for

TABLE I. Ionization rates $\Gamma(\sec^{-1})$ obtained from Eq. (22) at $\lambda=1064$ nm, $E_0=0.053$ a.u. ($I=10^{14}$ W/cm^2). All parameters are in a.u.

R	4	6	7.5	9.5	14
Δ	0.1	0.0176	0.007	0	0
ER	0.2	0.3	0.4	0.5	0.7
$\frac{\pi}{4}\delta$	1.72	0.036	0.005	0	0
$P_\pm$	0.18	0.96	1	1	1
$\Gamma(\beta=0)$	0.8×10^{12}	2×10^{13}	1×10^{13}	4×10^{13}	8×10^{12}
$\Gamma(\beta=0.1)$	0.2×10^{12}	2×10^{13}	1×10^{13}	3×10^{13}	2×10^{12}

triatomics [10]. Around this critical distance R_c, the Rabi frequency, $\omega_R=\mu(R)E$, which is also equal to the Stark energy displacement of the LUMO from its field-free value, dominates, i.e., $\omega_R>\varepsilon_{1\sigma_u}-\varepsilon_{1\sigma_g}$. Beyond this distance, the LUMO, ε_+, becomes trapped in the upper well created by the field and approaches the behavior of a single atomic orbital in the field, Fig. 4 [35].

IV. ADIABATIC-DIABATIC EVOLUTION

As described in Sec. IV, symmetric molecular ions differ from atoms due to the presence of HOMO's and LUMO's which are strongly coupled by the radiation field through the interaction $\mu(R)\ E(t)$, where $\mu(R)$ is the electronic transition moment between the two doorway molecular orbitals. $\mu(R)$ diverges linearly as R for orbitals which are quasidegenerate at large distances [3,13]. Thus in the case of one valence electronic diatomic molecules, a pair of HOMO's and LUMO's are the essential states, e.g., $1\sigma_g$ and $1\sigma_u$ in H_2^+. One can therefore treat the system as a two-level system for the population transfer between the HOMO and the LUMO. Our previous calculations [14] showed that the population difference between the HOMO and the LUMO follow the field for large R such that the Rabi frequency $\omega_R=\mu(R)E=ER/2$ for H_2^+ is larger than the energy separation $\Delta\varepsilon=\varepsilon_{1\sigma_u}-\varepsilon_{1\sigma_g}$. As an example at $R=6$ a.u., $\Delta\varepsilon=0.48$ eV$=0.0176$ a.u., whereas $\omega_R=0.16$ a.u., at $I=10^{14}$ W/cm^2 i.e., ten times larger than the energy separation between the LUMO and the HOMO.

The two-level system in the presence of a time-dependent field was studied in detail by Kayanuma [36] as a transfer-matrix problem at near crossings of the field-modified electronic states $\varepsilon_\pm$ illustrated in Fig. 5. Exact equations for these states without ionization as a function of R and t were described in Ref. [37]. The relevant parameter which describes population of these states as a function of time is the adiabacity parameter

$$\delta(t,R)=\frac{[\Delta\varepsilon(R)]^2}{\omega E(t)\mu(R)}, \tag{20}$$

which defines the transition probability between the field adiabatic states $\varepsilon_\pm(t)$. At the maximum of the field, i.e., at periods $\tau=\pi/2\omega$ (quarter cycles), then $E(t)=E=(8\pi/cI)^{1/2}$, and $\varepsilon_\pm$ are the static field states illustrated in Fig. 4. The transition probability between these states, called the nonadiabatic transition probability, can be reduced to a Landau-Zener type of equation [37,38],

$$P_\pm(t,R)=\exp[-\pi\delta(t,R)/4]. \tag{21}$$

In Table I we calculate the values of various parameters and of $P_\pm$ for peak values of the field at $I=10^{14}$ W/cm^2, i.e., $E_0=0.043$ a.u., as a function of R assuming $\mu(R)=R/2$. We observe in this table the rapid rise of the excitation of the LUMO, ε_+, between 4 and 6 a.u., in agreement with the static field ionization rates $\Gamma_\pm$ (Fig. 6) and the time dependent rates (Figs. 2 and 3). In the region of large $R>6$, where the ionization plateau and hence CREI occurs, $P_\pm\cong1$, corresponding to the diabatic regime [14,15]. This is the range where $\omega_R>\Delta\varepsilon$; then it can be shown that $P_\pm=1/2$, on average [14], since ε_+ and ε_- both become upper or lower adiabatic states for opposite phases of the field. One can therefore expect that the ionization rate averaged over a large number of cycles will be $\Gamma=\frac{1}{2}\Gamma_+$, or, more precisely,

$$\Gamma=\tfrac{1}{2}[P_\pm\Gamma_+ +(1-P_\pm)\Gamma_-], \tag{22}$$

where $\Gamma_\pm$ are the maximum static (peak) field ionization rates illustrated in Fig. 4. In Table I we have calculated the expected ionization rates $\Gamma(\sec)=\Gamma(\text{a.u.})\times(2.4\times10^{17})$ from the values of $\Gamma_\pm$, i.e., the static field ionization rates of the LUMO and the HOMO, $\varepsilon_\pm$. We note that the agreement between these adiabatic ionization rates calculated at the peak of the field and the time-dependent results illustrated is for both magnetic fields, $\beta=0$ (Fig. 2) and $\beta=0.1$ (Fig. 3) quite satisfactory.

V. CONCLUSION

We have presented highly accurate numerical procedure, based on adaptive moving grids, to elucidate further the mechanism of charge-resonance-enhanced ionization in the one-electron prototype molecule H_2^+. Imposing a large magnetic field parallel to the internuclear axis and laser-field direction confines the electron along that axis, suppressing excitation into large orbit excited states. The effect of the magnetic field allows for control of the Stark energy shifts of the LUMO. This results in a displacement of the critical distance R_c for enhanced ionization to shorter distances with increasing magnetic-field strength (Fig. 3).

Population of the LUMO by the time-dependent laser field based on a Landau-Zener nonadiabatic model [Eq. (21)] followed by ionization at the peak of the laser field [Eq. (22)], gives reasonable agreement with the exact TDSE results for both zero and large magnetic fields. Such a model nevertheless needs to be generalized in order to take into account the long-range divergent radiative coupling between the HOMO and the LUMO due to charge-resonance effects, especially at the one- and three-photon resonances between these doorway states [3,39]. As noted above, ADK-type tunneling calculations for molecular ionization near equilibrium distances [34,35] work as well for molecules as for atoms since excitation and population of the LUMO is negligible (Table I). It is in the CREI region, $R \cong R_c$, where most efficient (complete) excitation of the LUMO occurs, and the above-barrier ionization or below-barrier trapping of this orbital and consequent ionization suppression explains very well the enhanced ionization in intense laser fields for both zero and large magnetic fields in this region of internuclear distances. We are currently extending moving grid methods for two electrons ionization in H_2, where it has now been shown that ionic molecular states H^+H^- are the main doorway states for enhanced ionization [40].

ACKNOWLEDGMENTS

We thank the Natural Sciences and Engineering Research Council of Canada (NSERC) and the Canadian Institute for Photonic Innovation (CIPI) for funding of this research.

[1] J. R. Hiskes, Phys. Rev. **122**, 1207 (1961).
[2] G. R. Hanson, J. Chem. Phys. **62**, 1161 (1975).
[3] A. D. Bandrauk, *Molecules in Laser Fields* (Dekker, New York, 1994), Chap. 1.
[4] C. S. Warke and A. K. Dutta, Phys. Rev. A **6**, 1747 (1977).
[5] Int. J. Quantum Chem. **64** (1997) (see references therein).
[6] T. Zuo, S. Chelkowski, and A. D. Bandrauk, Phys. Rev. A **48**, 3837 (1993).
[7] T. Zuo and A. D. Bandrauk, Phys. Rev. A **52**, 2511 (1995).
[8] S. Chelkowski and A. D. Bandrauk, J. Phys. B **28**, L723 (1995).
[9] A. D. Bandrauk, Comments At. Mol. Phys. **1(3)D**, 97 (1999).
[10] A. D. Bandrauk and J. Ruel, Phys. Rev. A **59**, 2153 (1999).
[11] K. Codling, L. J. Frasinski, and P. A. Hatherly, J. Phys. B **22**, L321 (1989).
[12] T. Seidemann, M. Y. Ivanov, and P. B. Corkum, Phys. Rev. Lett. **75**, 2819 (1995).
[13] R. S. Mulliken, J. Chem. Phys. **7**, 20 (1939).
[14] T. Zuo, S. Chelkowski, and A. D. Bandrauk, Phys. Rev. A **49**, 3943 (1994).
[15] A. D. Bandrauk and H. Yu, Phys. Rev. A **59**, 539 (1999).
[16] J. C. Slater, *Quantum Theory of Molecules and Solids* (McGraw Hill, New York, 1963), Vol. 1.
[17] P. B. Corkum, Phys. Rev. Lett. **71**, 1994 (1993); **62**, 1259 (1989).
[18] A. Scrinzi, M. Geissler, and T. Brabec, Phys. Rev. Lett. **83**, 706 (1999).
[19] D. Bauer and P. Mulser, Phys. Rev. A **59**, 569 (1999).
[20] T. Zuo, A. D. Bandrauk, M. Ivanov, and P. B. Corkum, Phys. Rev. A **51**, 3991 (1995).
[21] T. Zuo and A. D. Bandrauk, J. Nonlinear Opt. Phys. Mater. **4**, 533 (1995).
[22] D. B. Milosevic and A. F. Starace, Phys. Rev. Lett. **82**, 2653 (1999); Phys. Rev. A **60**, 3160 (1999).
[23] J. S. Heyl and L. Hernsquist, Phys. Rev. A **58**, 3567 (1998).
[24] S. Chelkowski, T. Zuo, and A. D. Bandrauk, Phys. Rev. A **46**, 5342 (1992).
[25] A. D. Bandrauk and H. Shen, J. Chem. Phys. **99**, 1185 (1993).
[26] S. Chelkowski, T. Zuo, O. Atabek, and A. D. Bandrauk, Phys. Rev. A **52**, 2977 (1995).
[27] H. Yu and A. D. Bandrauk, J. Chem. Phys. **102**, 1257 (1995).
[28] Z. Mulyukov, M. Pont, and R. Shakeshaft, Phys. Rev. A **54**, 4299 (1996).
[29] F. Gygi and G. Galli, Phys. Rev. B **52**, R2239 (1995).
[30] I. Kawata and H. Kono, J. Chem. Phys. **111**, 9498 (1999).
[31] V. Druskin and S. Moskow, Math. Comp. (to be published).
[32] H. Z. Lu, and A. D. Bandrauk (unpublished); L. D. Landau and E. M. Lifshitz, *Fluid Mechanics* (Pergamon, Oxford, 1987), Vol. 6.
[33] A. D. Bandrauk and H. Yu, J. Phys. B **31**, 4243 (1998); Phys. Rev. A **59**, 539 (1999).
[34] A. Talebpour, A. LaRochelle, and S. L. Chin, J. Phys. B **30**, L245 (1997); **31**, L49 (1998); Laser Phys. **7**, 851 (1997); A. Talebpour, Ph.D. thesis, Université Laval, 1998 (unpublished).
[35] M. J. DeWitt and R. J. Levis, Phys. Rev. Lett. **81**, 5701 (1998).
[36] Y. Kayanuma, Phys. Rev. A **50**, 843 (1994); **55**, R2495 (1997).
[37] I. Kawata, H. Kono, and Y. Fujimura, Chem. Phys. Lett. **289**, 546 (1998).
[38] J. F. McCann and A. D. Bandrauk, Phys. Lett. A **151**, 509 (1990).
[39] E. Aubanel and A. D. Bandrauk, Phys. Rev. A **48**, 2145 (1993).
[40] I. Kawata, H. Kono, and A. D. Bandrauk, Phys. Rev. A (to be published).